Visualization of Electronic Multiple Ordering and Its Dynamics in High Magnetic Field: Evidence of Electronic Multiple Ordering Crystals

Zhigao Sheng,*[†,‡,§,∇] Qiyuan Feng,[†,‡,∇] Haibiao Zhou,[†,‡,∇] Shuai Dong,[∥] Xueli Xu,[†] Long Cheng,[†] Caixing Liu,[†] Yubin Hou,[†] Wenjie Meng,[†,‡] Yuping Sun,[†,§,⊥] Masao Nakamura,[#] Yoshinori Tokura,[#,¶] Masashi Kawasaki,[#,¶] and Qingyou Lu*[†,‡,§]

[†]Anhui Key Laboratory of Condensed Matter Physics at Extreme Conditions, High Magnetic Field Laboratory and Hefei Science Center, and [⊥]Institute of Solid State Physics, Chinese Academy of Sciences, Hefei 230031, China

[‡]Hefei National Laboratory for Physical Sciences at Microscale, University of Science and Technology of China, Hefei 230026, China

[§]Collaborative Innovation Center of Advanced Microstructures, Nanjing University, Nanjing 210093, China

[∥]School of Physics, Southeast University, Nanjing 211189, China

[#]RIKEN Center for Emergent Matter Science (CEMS), Wako, Saitama 351-0198, Japan

[¶]Department of Applied Physics and Quantum Phase Electronics Research Center (QPEC), University of Tokyo, Tokyo 113-8656, Japan

S *Supporting Information*

ABSTRACT: Constituent atoms and electrons determine matter properties together, and they can form long-range ordering respectively. Distinguishing and isolating the electronic ordering out from the lattice crystal is a crucial issue in contemporary materials science. However, the intrinsic structure of a long-range electronic ordering is difficult to observe because it can be easily affected by many external factors. Here, we present the observation of electronic multiple ordering (EMO) and its dynamics at the micrometer scale in a manganite thin film. The strong internal couplings among multiple electronic degrees of freedom in the EMO make its morphology robust against external factors and visible via well-defined boundaries along specific axes and cleavage planes, which behave like a multiple-ordered electronic crystal. A strong magnetic field up to 17.6 T is needed to completely melt such EMO at 7 K, and the corresponding formation, motion, and annihilation dynamics are imaged utilizing a home-built high-field magnetic force microscope. The EMO is parasitic within the lattice crystal house, but its dynamics follows its own rules of electronic correlation, therefore becoming distinguishable and isolatable as the electronic ordering. Our work provides a microscopic foundation for the understanding and control of the electronic ordering and the designs of the corresponding devices.

KEYWORDS: *electronic multiple ordering, high magnetic field, magnetic force microscopy, antiferromagnetic phase, manganite, phase separation*
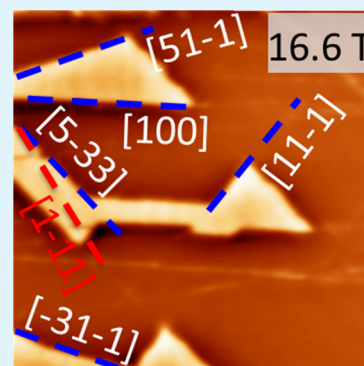
INTRODUCTION

Solid, liquid, gas, and a few other phases are the basic forms of matter, where the key points for the emergence of multiple phases are symmetry breaking and the accompanying order-parameters.[1,2] In solid, the symmetries of lattice and electrons can act as order-parameters for the formation of phases. Long-range ordered atomic lattice produces the lattice crystal. Electrons, however, have multiple degrees of freedom including charge, orbital, and spin. Each of these quantities can form a distinct type of long-range ordering, giving rise to an electronic crystal.[2,3] In other words, the long-range electronic ordering based on ferromagnetic (FM) spin order, anti-FM (AFM) spin order, orbital order (OO), or charge order (CO) should be expected, and indeed, they have been confirmed.[3–6] Among

them, the FM ordering has already been studied extensively on both the macroscopic and microscopic length scales.[4–9] For the remaining types, they have not been intensively studied before but are attracting more attention recently because of the crucial roles they play in electronic materials, especially in novel phenomena including high-temperature superconductivity, topological edge/surface state, giant and colossal magneto-resistance effects, and so forth.[10–13]

To date, a vast majority of the studies on these remaining types have been performed in momentum space using
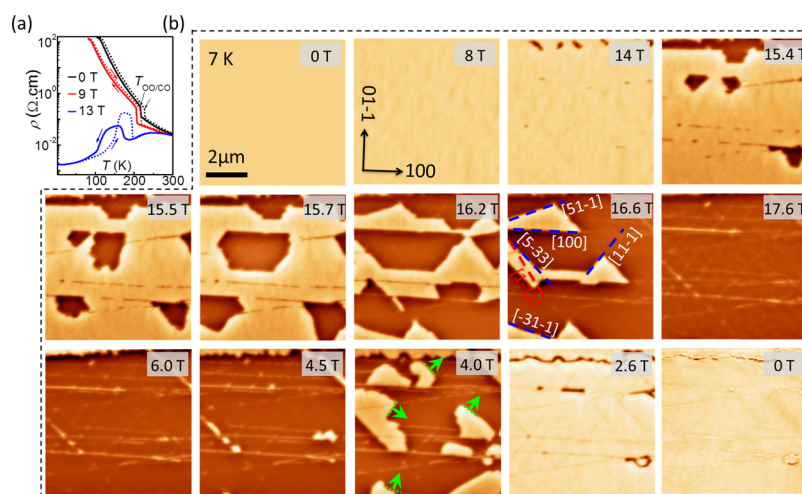
Figure 1. EMO dynamics in the PCMO film. (a) Temperature dependence of resistivity (ρ) for the PCMO film measured at 0, 9, and 13 T. The magnetic field was applied along the out-of-plane direction, and the resistivity was measured along the [100] direction. (b) Selected MFM images, with $7 \times 7 \ \mu m^2$ in size, showing the annihilation and formation of the AFM/OO/CO phase. The sample was initially cooled from room temperature to 7 K, and then, the magnetic field was swept up to 17.6 T and back down to zero. The green lines and arrows are marked for the phase boundaries and their movement directions during the phase dynamics. The color scales of all the images in this letter have been adjusted to clarify the contrast (see details in Method S2).

macroscopic techniques, such as neutron diffraction and X-ray diffraction.[8−10] Limited microscopic investigations, especially the real-space imaging of the electronic ordering, have been done under fairly static conditions, including the atomically resolved imaging of the AFM in NiO using a magnetic exchange force microscope, the imaging of the static AFM domains by X-ray magnetic linear dichroism spectromicroscopy, and so forth.[14−17] It is notable that most of the electronic ordering patterns imaged look irregular, and their boundaries and dynamic behaviors are usually determined by nonintrinsic factors such as sample shape, surface/interface, strain, and defects. This implies that not only the intrinsic characteristics associated with the long-range order of the electronic degree of freedom are missing, but also the task of distinguishing or isolating the electronic ordering out from the lattice crystal is difficult.[5,6]

In addition to the simple electronic ordering, a special category also exists in which multiple electronic parameters are in long-range orders simultaneously. It can be named as electronic multiple ordering (EMO).[8−10] To the best of our knowledge, although there have been macroscopic investigations,[9,10] no microscopic study on EMO has been carried out. The reasons can be attributed to the following two difficulties: (1) EMO often involves AFM and/or OO orders, which have no appropriately detectable parameters. For instance, the net magnetic moment of each AFM domain is approximately equal to zero,[18,19] which tremendously reduces the possibility for an AFM domain to be detected. The situation is even worse for the OO case. (2) A panoramic observation of the generation and annihilation processes of the EMO phase generally needs extreme conditions, such as high magnetic field, because of the robustness of the multiple orderings.

Here, we cope with these two issues by utilizing a 20 T high magnetic field variable temperature magnetic force microscopy (MFM) system of high stability and sensitivity.[20,21] The EMO and its dynamics, featured with well-defined boundaries and specific cleavage planes, are visualized microscopically. The EMO boundaries can only be found along four specific axes, on which the charge and orbital of electrons are ferroically ordered

in a CE-type antiferroic electronic crystal. Moreover, these electronic phase boundaries move in parallel during their growth or annihilation in the process of varying magnetic field or temperature. These observations provide the evidence of the EMO showing its intrinsic crystallographic nature, which also implies that although parasitized in the house of atomic crystal lattice, the EMO follows its own intrinsic rules of electronic correlations.

■ EXPERIMENTAL SECTION

The EMO sample considered in this work is a 30 nm thick half-doped $Pr_{1/2}Ca_{1/2}MnO_3$ (PCMO) thin film, which was grown on a substrate of $(LaAlO_3)_{0.3}(SrAl_{0.5}Ta_{0.5}O_3)_{0.7}(011)$ (LSAT) via pulsed laser deposition.[22] This epitaxial film is of a single lattice crystal domain only without twins, as confirmed by the X-ray reciprocal mapping (Figure S1). The ground state of PCMO is an AFM arrangement, consisting of the FM Mn zigzag chains below the Néel temperature T_N, known as the CE-type structure.[8,9] At the same time, PCMO has an equal number of Mn^{3+} and Mn^{4+} cations, resulting in concomitant charge ordering and orbital ordering of the Mn^{3+} $d_{3x^2−r^2}$ and $d_{3y^2−r^2}$ orbitals. Thus, the multiple quantum orders of AFM, OO, and CO co-exist simultaneously in the sample, which offers an ideal platform for the study of EMO. In bulk PCMO, the minimum magnetic field required to fully melt the AFM/OO/CO phase is as high as 27 T at 1.4 K,[23,24] which is far beyond the scope of any current imaging tool. However, it is reduced to below 20 T in the case of thin film because of the enhanced electron itinerancy.[26] Although this field is still too strong for most of imaging tools, it does permit our home-built 20 T MFM system to perform the first microscopic imaging on the phase dynamics of the robust CE-type AFM/OO/CO crystal (see Method S2).

When cooled down, the PCMO film undergoes an OO/CO transition at $T_{OO/CO} = 220$ K,[23] as indicated by the sharp increase in resistivity Figure 1a, which suggests high quality of the PCMO thin film (Figure S2). Applying a 9 T magnetic field shifts the transition to a slightly lower temperature, whereas at 13 T, the CO is greatly suppressed, and interestingly, it is only present within a temperature range of 100−200 K, indicating a reentrance behavior when the sample is warmed after the field-cooling process.[25,26] To visualize the EMO and its dynamics in the PCMO film, high-field MFM measurements were carried out at various temperatures and magnetic fields. In this work, the applied magnetic fields were always perpendicular to the film
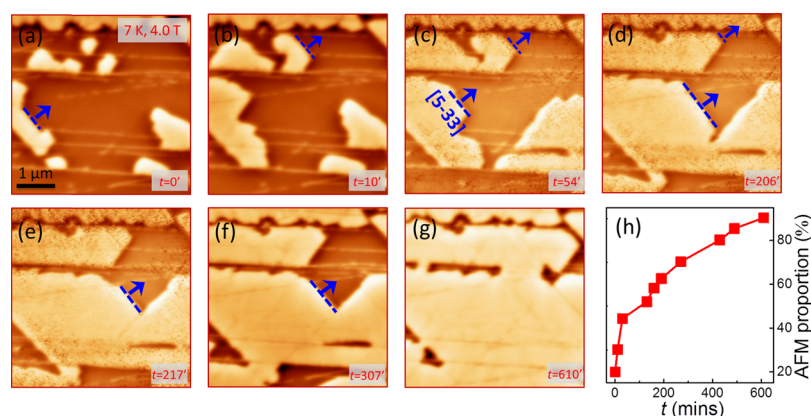
Figure 2. Relaxation behaviors of AFM/OO/CO multiple ordering. (a–g) MFM images taken at different times (t = 0, 10, 20, 75, and 110 min) at 7 K when the applied magnetic field was swept down and fixed at 4.0 T. All images are 6×6 μm^2 in size. The blue lines and arrows indicate the phase boundaries and their moving directions during the phase dynamics along [5−33]. (h) time dependence of the AFM areal proportion obtained from the MFM images for the time relaxation process at 4.0 T [partially shown in (a−g)].

surface. Figure 1b shows the representative MFM images recorded during the field-increasing and decreasing processes at 7 K (see more images in Figure S3 and Movie S1). The bright and dark regions in the images correspond to the phase domains that exert different force gradient on the tip, and they correspond to the AFM/OO/CO phase (negligible force) and field-induced FM (FFM) phase (attractive force), respectively. The color scales of all the images in this letter have been adjusted to clarify the contrast (see details in Method S2). In zero and low magnetic fields, the AFM/OO/CO phase remains very stable, and the MFM images taken below 14 T are nearly the same. At 14 T, several dark droplets begin to appear at the top of the images, indicating the nucleation of the FFM phase. After further increase of the magnetic field, the FFM phase domains become larger and mutually connected. The nucleation and growth of the FFM phase correspond to the destruction (melting) of the AFM/OO/CO phase. When the magnetic field reaches 17.6 T, almost the whole image appears dark, because the entire AFM/OO/CO phase is transformed into the FFM phase with some bright lines remaining. Once the magnetic field is reduced from 17.6 T, the FFM phase remains unchanged, until the field is below 6 T. At 4.5 T, the AFM/OO/CO seeds emerge. When the field is reduced further, the AFM/OO/CO phase expands and the FFM phase shrinks. In the end, with the magnetic field being below 2.6 T, almost all the PCMO is occupied by the AFM/OO/CO phase. The areal proportion of the AFM/OO/CO phase in the MFM images and the corresponding electrical resistivity are compared (Figure S3). Both the microscopic areal data and the macroscopic electrical transport data show hysteretic behaviors and the hysteresis loops are in good agreement.

The most remarkable discovery in Figure 1b is that an AFM/OO/CO phase domain behaves like a single-crystal lattice in both the destruction and reconstruction processes. The transition of the AFM/OO/CO phase follows some well-defined polygon geometry with sharp boundary lines (Figure S4). With the increasing of the magnetic field, a FFM phase domain grew into trapezoid shape around 15.7 T and a triangularly shaped AFM/OO/CO phase domain emerged at 16.6 T. Similar phenomena occur in all the MFM images of the AFM/OO/CO dynamics, that is, these specific boundary lines were formed not only in the growth but also in the annihilation process and not only in the final but also in the middle state of a phase domain. It is interesting to find that these phase-domain boundary lines align completely and exclusively along the following five axes: [11−1], [−31−1], [51−1], [5−33], and [100], in the pseudo-cubic coordination (dashed blue lines in Figure 1b, 16.6 T), which will be discussed further in below.

Another important phenomenon observed here is the relaxation behavior. During the field sweeping process at 7 K, MFM images were taken as a function of time. Figure 2a−g presents the typical results, which were obtained when the applied magnetic field was swept down and fixed at 4.0 T. It is found that the EMO phase domains grow with time and the relaxation process is quite slow. For example, the occupancy of the EMO (defined as the areal ratio of the AFM/OO/CO area to the area of the whole image) is only 20% at t = 0. It expands slowly, and its occupancy increases from 48% at t = 54 min Figure 2c to 67% at t = 217 min (Figure 2e). It grows to as large as 90% after about 10 h (Figure 2g). This slow relaxation process can be found quantitatively in Figure 2h, in which the time dependence of the EMO occupancy is displayed. Besides, the relaxation behaviors show strong diversity in the EMO dynamics during both field-driven and temperature-driven phase transition processes (Figure S6). These slow and diverse relaxation characteristics imply that the interactions among the co-existing quantum orders in the PCMO film are rather subtle and their competitions with the disordered state are well-balanced near the phase transition.[29] It should be noted that such relaxation characteristics of the EMO are similar to the lattice crystal relaxation behavior observed in equilibrium.[30]

In the MFM images shown above, in addition to the bright and dark territories, several straight lines, showing weak magnetic field dependence, exist with relatively bright color. They are also present in the topography and are ascribed to crosshatching lines (CHLs) originating from the strain relaxation of the film (Figure S4). It is found that these CHLs also align completely and exclusively along the five axes [11−1], [−31−1], [51−1], [5−33], and [100] in the pseudo-cubic coordination. In the PCMO film studied here, there exist two kinds of the strains, which may relate to the formation of the CHLs. On the one hand, the epitaxial strain due to the mismatch between the substrate and film is the main contributor. With the relaxation of epitaxial strain force, CHLs emerge on the film surface.[27,28] For the substrate with cubic lattice structure, almost all previously observed CHLs are along the axes with low Miller indices, such as cubic [110] and [100]. In the PCMO film, the CHL along [100] belongs to this category (Figure S4). On the other hand, the CHLs with relatively high Miller indices, such as cubic [11−1], [−31−1], [51−1], and [5−33], might come from the accommodation strain induced by electronic phase transition. As a typical strongly correlated electron system, the formation of the AFM/OO/CO multiple-ordered phase in the PCMO is accompanied by an atomic lattice deformation. This atomic lattice deformation happens not only in bulk but also in thin film samples (Figure S4). As a result, such electronic phase transition-induced deformation can produce an accommodation strain in the PCMO film in addition to the substrate-induced epitaxial strain. The exclusive existing of the CHLs with relatively high Miller indices implies that the electronic phase transition obeys some kinds of electronic correlation rules, which will be discussed further below.

As shown in Figure 1b, it is found that the EMO grows up from and spreads toward the CHLs, which act as their start points and eventual boundaries. Because of the inhomogeneity of lattice structure and
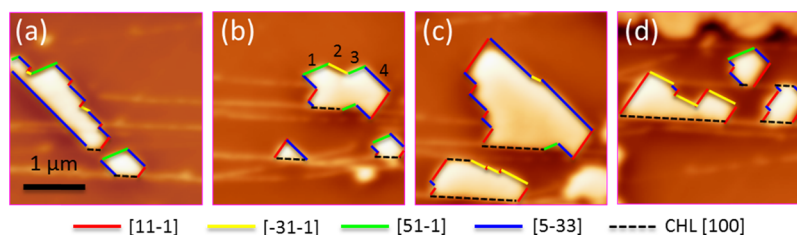
Figure 3. Domain structure of EMO within the CHL-free region. (a−d) Selected MFM images, taken at different magnetic fields at 7 K with 3.2 × 3.2 μm^2 in size, showing the AFM/OO/CO phase domain structure. The magnetic field was swept up to 17.6 T and back down to zero, and these MFM images were taken when the applied magnetic field was swept down.
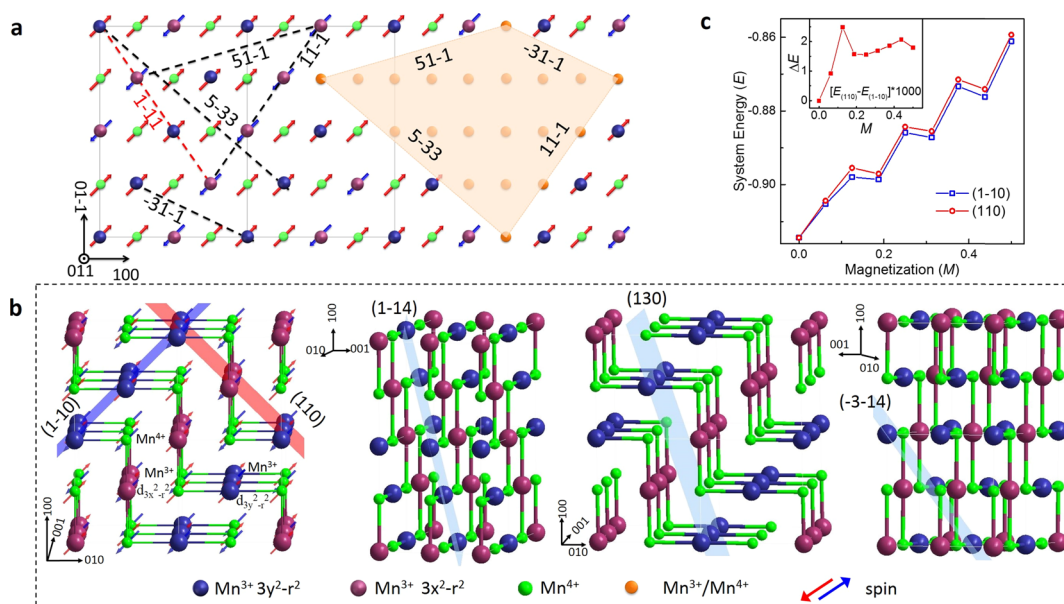

Figure 4. Charge and orbital configurations of the CE-type AFM/OO/CO in PCMO. (a) Schematic of the CE-type AFM/OO/CO structure on the (011) surface of the PCMO film. On the black dashed lines, along [11−1], [−31−1], [51−1], and [5−33], respectively, the manganese ions have multiple ferroic ordering, that is, the spin, orbit, and charge of manganese ions are exactly same on these lines (FOLs). Remarkably, these FOLs are consistent with the AFM/OO/CO phase domain boundaries of PCMO film as shown in Figure 2b, schematics of the CE-type AFM/OO/CO structure of the PCMO film. The blue sheets correspond to the (1−10), (130), (1−14), and (−3−14) planes, respectively. In addition to (1−10), the (110) plane was also highlighted in first image of (b). Both (1−10) and (110) plane have identical atomic crystal, charge, and spin configurations but different orbital ordering. The (1−10) plane is ferro-orbital, while the (110) plane shows zigzag orbital configuration. Pseudo-cubic coordination symmetry was used in (a,b). (c) Difference of the energy of the systems, which contained either the (1−10) plane or (110) plane as phase domain boundaries.

energy scale on the CHLs, it is better to pay more attention on the EMO dynamics within the territories surrounded by the CHLs, that is, CHLs-free regions. Figure 3 presents the typical MFM images taken at 7 K with different magnetic fields, showing the EMO domain structure in the middle stage, in which most phase domain boundaries are located in the CHL-free region. In the CHL-free region, there are several characters need to be emphasized as follows.

(1) Even in the CHLs-free regions, the EMO domains still follow some well-defined polygon geometry with sharp boundaries. For example, as shown in the Figure 3b, the phase boundaries 1, 2, 3, and 4 are not on the CHLs but still show straight-line-like behavior.

(2) What's more, these electronic phase domain boundary lines, existing in the CHLs-free regions, also align completely and exclusively along the four axes [11−1], [−31−1], [51−1], and [5−33] in the pseudo-cubic coordination (color lines in Figure 3), which are exactly the same as the high Miller indices of the CHLs. This implies that both the EMO domains in the CHL-free regions and the formation of the high Miller index CHLs stem from the electronic correlation rules.

(3) It is important to notice that the directions of these domain boundaries in the CHL-free regions do not copy the directions

of the neighboring CHLs. For instance, the phase boundary lines 1, 2, 3, and 4 in Figure 3b are along [51−1], [−31−1], [51−1], and [5−33], respectively. However, the nearest neighboring CHLs for these boundaries are along [100]. Such discrepancy between electronic phase boundaries and neighboring CHLs indicates that the directions of the CHLs do not affect the formation of EMOs so strongly. In other words, the dynamics of EMOs within the CHL-free regions can be independent of the CHLs. Actually, similar phenomena occur almost in all the MFM images of EMOs, that is, these specific boundary lines were formed not only in the growth but also in the annihilation process and not only in the final but also in the primary and middle states of the phase domain.

(4) In the CHL-free regions, the dynamic process exhibits that the EMO boundaries can move without changing their directions. As shown in the Figure 2c−f, the blue line and arrow indicate how an EMO boundary moves without changing its direction along [5−33], causing the disordered phase (dark color) to shrink step by step. This feature is one of the intrinsic crystallographic characteristics of EMOs and can happen independently in a CHL-free region without atomic lattice

crystal boundaries, implying again that the observed EMOs follow its own rules of electronic correlation.

(5) One point deserving special attention is that several phase domain boundaries have relatively large crystal Miller indices (such as [5−33] axis). The distances between the nearest atoms on these lines and planes are several times larger than the unit cell size. This may indicate that the formation and dynamics of the EMOs are governed by the electronic correlations, which can be even beyond the range of a lattice unit cell.

These characters are quite different from the phase domain images observed in other materials, which indicate that the EMO domain studied here is not only an electronic phase (note: an electronic phase may have irregular shape) but also show crystalline structure and behavior. To better understand the multiple-ordered electronic crystal, it is of central importance to clarify the relationship between the electronic correlation rules and those special phase boundaries with high Miller indices. Figure 4a shows the (011) section (film surface) view of the CE-type AFM/OO/CO ordering. It is found that these four axes with high Miller indices (i.e., [11−1], [−31−1], [51−1], and [5−33]) are unique because the spin, orbital, and charge of manganese atoms on them are the same, that is, ferroic ordering of spin, orbital, and charge. Moreover, these four axes are the only four ferroic ordering lines (abbreviated as FOLs) in the unit cell of the (011) plane with the CE-type structure. In fact, careful investigation shows that there are four, and only four, crystal planes [namely, the (1−10), (130), (1−14), and (−3−14) planes] in the CE-type EMO of the PCMO (Figure 4b), each of which contains identical orbital and charge at each lattice site, that is, manganese ions on those planes have ferroic ordering of orbital and charge (ferroically ordered planes, abbreviated as FOPs). These four planes intersect with the film surface, namely the (011) plane, and produce the four axes [11−1], [−31−1], [51−1], and [5−33], respectively. We emphasize that these are exactly the same as the FOLs, the high Miller indices CHLs, and the EMO boundaries within the CHL-free regions (Figure 2).

From lattice viewpoint, the (110) and (1−10) planes are equivalent (Figure 4b), but they are not if the charge and orbital degrees of freedom are taken into account (Figure 4a). These planes intersect with the film surface along the axes [1−11] and [11−1], respectively. Because the (1−10) plane is an FOP, the [11−1] axis it produces is an FOL. However, the [1−11] axis, which is produced by a non-FOP (110), is not an FOL (Figure 4a). In all the MFM images we obtained, only the FOL [11−1] can be found as a phase boundary, whereas the non-FOL [1−11] is absent. To better understand this issue, we have done the theoretical simulation as shown in Method S3, Figure S5. The energy of the whole system (E) is recorded as a function of magnetization (M) by considering both FOP (1−10) and non-FOP (110) as phase boundaries. It is found that the energy depends substantially on the boundary type. As shown in Figure 4c, the theoretical simulation reveals that the energy of the electronic system containing the FOP (1−10) as domain boundaries is lower than that containing non-FOP (110) as domain boundaries, which is consistent with our experimental observation as shown in Figures 1 and 3.

With the boundaries being determined by the sharp and specific FOLs and FOPs, an EMO phase domain in the PCMO film behaves just like a single crystal of the lattice type. Its nucleation, growth, coalescence, and collapse in the background of disordered phase is much like the corresponding processes exhibited by a single crystal of the lattice type in the melt (ice in water, for instance). From this point of view, the EMO observed here is a kind of electronic crystal and the FOPs and FOLs are the cleavage planes and crystal edges, respectively. On the basis of the distributions of spin, charge, and orbital in the FOPs and FOLs, we can conclude that the quantum orders, or more precisely, OO/CO, govern the formation and dynamics of the CE-type EMO in the PCMO film. This feature not only reveals the crystallographic behavior of the EMO but also evidences that although the EMOs are parasitic within the lattice crystal house their dynamics follow their own intrinsic rules of electronic correlation.

CONCLUSIONS

In summary, we have visualized the structure and phase dynamics of the EMO in a manganite thin film at the microscopic scale utilizing a high magnetic field MFM. Five types of critical lines on the surface, govern the entire dynamics of the EMO, making it behave like an electronic crystal. Although the EMO is parasitic inside the lattice sites, the presence of the specific lines and planes indicates that such a category of electronic crystal has its own unique crystalline rules. Its dynamics and boundary behaviors are intrinsic and depend mainly on the coupling among the multiple-ordered electronic degrees of freedom themselves. This is the first direct observation of the intrinsic crystallographic characteristics of EMO, which is crucial in further understanding the phase dynamics and device involving mutually interacted electron orderings.

ASSOCIATED CONTENT

Ⓢ Supporting Information

The Supporting Information is available free of charge on the ACS Publications website at DOI: 10.1021/acsami.8b04057.

> Reciprocal space maps around the (222) and (310) reflections of $Pr_{0.5}Ca_{0.5}MO_3$ (PCMO) film; the comparison of X-ray diffraction, electrical transport, and MFM morphology for two kinds of PCMO thin film samples; the resistivity, MFM images, and AFM/OO/CO areal proportions of PCMO film as a function of magnetic field within scanning filed up and down; lattice deformation and domain boundaries of PCMO films; model study on phase interfaces and an example of phase separated domains; and relaxation behaviors of AFM/OO/CO electronic crystals (PDF)
> MFM images taken at 7 K (AVI)

AUTHOR INFORMATION

Corresponding Authors
*E-mail: zhigaosheng@hmfl.ac.cn (Z.G.S.).
*E-mail: qxl@ustc.edu.cn (Q.Y.L.).
ORCID ⓘ
Shuai Dong: 0000-0002-6910-6319
Qingyou Lu: 0000-0003-1934-8165
Author Contributions
▽Z.S., Q.F., and H.Z. contributed equally to this work.
Notes
The authors declare no competing financial interest.

ACKNOWLEDGMENTS

■ REFERENCES

(1) Mermin, N. D. Topological theory of defects in ordered media. *Rev. Mod. Phys.* **1979**, *51*, 591−648.

(2) Attfield, J. P.; Bell, A. M. T.; Rodriguez-Martinez, L. M.; Greneche, J. M.; Cernik, R. J.; Clarke, J. F.; Perkins, D. A. Electrostatically driven charge-ordering in Fe2OBO3. *Nature* **1998**, *396*, 655−658.

(3) Ishihara, S.; Inoue, J.; Maekawa, S. Effective Hamiltonian in manganites: Study of the orbital and spin structures. *Phys. Rev. B: Condens. Matter Mater. Phys.* **1997**, *55*, 8280−8286.

(4) Lu, Q.; Chen, C.-C.; de Lozanne, A. Observation of magnetic domain behavior in colossal magnetoresistive materials with a magnetic force microscope. *Science* **1997**, *276*, 2006−2008.

(5) Wu, W.; Israel, C.; Hur, N.; Park, S.; Cheong, S.-W.; De Lozanne, A. Magnetic imaging of a supercooling glass transition in a weakly disordered ferromagnet. *Nat. Mater.* **2006**, *5*, 881−886.

(6) Binnig, G.; Rohrer, H. Scanning tunneling microscopy. *IBM J. Res. Dev.* **2000**, *30*, 279−293.

(7) Cai, K.; Yang, M.; Ju, H.; Wang, S.; Ji, Y.; Li, B.; Edmonds, K. W.; Sheng, Y.; Zhang, B.; Zhang, N.; Liu, S.; Zheng, H.; Wang, K. Electric field control of deterministic current-induced magnetization switching in a hybrid ferromagnetic/ferroelectric structure. *Nat. Mater.* **2017**, *16*, 712−716.

(8) Jirák, Z.; Damay, F.; Hervieu, M.; Martin, C.; Raveau, B.; André, G.; Bourée, F. Magnetism and charge ordering in Pr0.5CaxSr0.5-xMnO3 (x=0.09 and 0.5). *Phys. Rev. B: Condens. Matter Mater. Phys.* **2000**, *61*, 1181−1188.

(9) van den Brink, J.; Khaliullin, G.; Khomskii, D. Charge and orbital order in half-doped manganites. *Phys. Rev. Lett.* **1999**, *83*, 5118−5121.

(10) Nogués, J.; Schuller, I. K. Exchange bias. *J. Magn. Magn. Mater.* **1999**, *192*, 203−232.

(11) Zhang, S.-C. A unified theory based on SO(5) symmetry of superconductivity and antiferromagnetism. *Science* **1997**, *275*, 1089−1096.

(12) Baibich, M. N.; Broto, J. M.; Fert, A.; Nguyen Van Dau, F.; Petroff, F.; Etienne, P.; Creuzet, G.; Friederich, A.; Chazelas, J. Giant Magnetoresistance of (001)Fe/(001)Cr Magnetic Superlattices. *Phys. Rev. Lett.* **1988**, *61*, 2472−2475.

(13) Kuwahara, H.; Tomioka, Y.; Asamitsu, A.; Moritomo, Y.; Tokura, Y. A First-Order Phase Transition Induced by a Magnetic Field. *Science* **1995**, *270*, 961−963.

(14) Kaiser, U.; Schwarz, A.; Wiesendanger, R. Magnetic exchange force microscopy with atomic resolution. *Nature* **2007**, *446*, 522−525.

(15) Shpyrko, O. G.; Isaacs, E. D.; Logan, J. M.; Feng, Y.; Aeppli, G.; Jaramillo, R.; Kim, H. C.; Rosenbaum, T. F.; Zschack, P.; Sprung, M.; Narayanan, S.; Sandy, A. R. Direct measurement of antiferromagnetic domain fluctuations. *Nature* **2007**, *447*, 68−71.

(16) Scholl, A.; Stöhr, J.; Lüning, J.; Seo, J. W.; Fompeyrine, J.; Siegwart, H.; Locquet, J.-P.; Nolting, F.; Anders, S.; Fullerton, E. E.; Scheinfein, M. R.; Padmore, H. A. Observation of antiferromagnetic domains in epitaxial thin films. *Science* **2000**, *287*, 1014−1016.

(17) Ma, E. Y.; Cui, Y.-T.; Ueda, K.; Tang, S.; Chen, K.; Tamura, N.; Wu, P. M.; Fujioka, J.; Tokura, Y.; Shen, Z.-X. Mobile metallic domain walls in an all-in-all-out magnetic insulator. *Science* **2015**, *350*, 538−541.

(18) García-Fernández, M.; Wilkins, S. B.; Lu, M.; Li, Q.; Gray, K. E.; Zheng, H.; Mitchell, J. F.; Khomskii, D. Antiferromagnetic domain structure in bilayer manganite. *Phys. Rev. B: Condens. Matter Mater. Phys.* **2013**, *88*, 075134.

(19) Dagotto, E.; Hotta, T.; Moreo, A. Colossal magnetoresistant materials: The key role of phase separation. *Phys. Rep.* **2001**, *344*, 1−153.

(20) Zhou, H.; Wang, L.; Hou, Y.; Huang, Z.; Lu, Q.; Wu, W. Evolution and control of the phase competition morphology in a manganite. *Nat. Commun.* **2015**, *6*, 8980.

(21) Okuyama, D.; Nakamura, M.; Wakabayashi, Y.; Itoh, H.; Kumai, R.; Yamada, H.; Taguchi, Y.; Arima, T.; Kawasaki, M.; Tokura, Y. Epitaxial-strain effect on charge/orbital order in Pr0.5Ca0.5MnO3 films. *Appl. Phys. Lett.* **2009**, *95*, 152502.

(22) Daoud-Aladine, A.; Rodríguez-Carvajal, J.; Pinsard-Gaudart, L.; Fernández-Díaz, M. T.; Revcolevschi, A. Zener polaron ordering in half-doped manganites. *Phys. Rev. Lett.* **2002**, *89*, 097205.

(23) Tokunaga, M.; Miura, N.; Tomioka, Y.; Tokura, Y. *Phys. Rev. B: Condens. Matter Mater. Phys.* **1998**, *57*, 5259−5264.

(24) Prellier, W.; Buzin, E. R.; Simon, C.; Mercey, B.; Hervieu, M.; de Brion, S.; Chouteau, G. High magnetic field transport measurements of charge-ordered Pr0.5Ca0.5MnO3 strained thin films. *Phys. Rev. B: Condens. Matter Mater. Phys.* **2002**, *66*, 024432.

(25) Yuan, Q.; Kopp, T. Charge ordering in half-doped Pr(Nd)-0.5Ca0.5MnO3 under a magnetic field. *Phys. Rev. B: Condens. Matter Mater. Phys.* **2002**, *65*, 174423.

(26) Shiryaev, S. Y.; Jensen, F.; Petersen, J. W. On the nature of cross-hatch patterns on compositionally graded Si1-xGex alloy layers. *Appl. Phys. Lett.* **1994**, *64*, 3305−3307.

(27) Kim, S. G.; Wang, Y.; Chen, I.-W. Strain relaxation in buried layer in (Ca1−xSrx)(Zr1−xRux)/SrRuO3/SrTiO3 system. *Appl. Phys. Lett.* **2006**, *89*, 031905.

(28) Sirena, M.; Steren, L. B.; Guimpel, J. Magnetic relaxation in bulk and film manganite compounds. *Phys. Rev. B: Condens. Matter Mater. Phys.* **2001**, *64*, 104409.

(29) Horcas, I.; Fernández, R.; Gómez-Rodríguez, J. M.; Colchero, J.; Gómez-Herrero, J.; Baro, A. M. WSXM: A software for scanning probe microscopy and a tool for nanotechnology. *Rev. Sci. Instrum.* **2007**, *78*, 013705.

(30) Slater, J. C.; Koster, G. F. Simplified LCAO method for the periodic potential problem. *Phys. Rev.* **1954**, *94*, 1498−1524.